NUMERICAL STUDY OF FLOWS IN THE VICINITY OF AIRFOIL TRAILING EDGE

Kazuhiro Nakahashi, Yuta Sakurai, and Aya Kitoh
Department of Aerospace Engineering, Tohoku University

Keywords: *Airfoil, Trailing edge noise*

Abstract

Flows around NACA0012 airfoil at relatively low Reynolds number are numerically simulated using the Building-Cube method which uses very fine Cartesian mesh. The computed results show that laminar boundary layer on upper surface of the airfoil separates at mid-chord and generates vortices that flows down along the airfoil surface. When a vortex reaches at the trailing edge, it generate a counter-rotating vortex due to the large pressure difference around the sharp trailing edge. At the same time a pressure wave is generated that propagates in all directions from the trailing edge with sonic velocity. Effects of small modifications of airfoil geometry near the trailing edge are also numerically investigated.

1 Introduction

Due to the development of quieter turbofan engines, airframe noise has recently become an important noise source in commercial aircrafts. The trailing edge of the leading-edge slat, especially, is reported to be a dominant high-lift noise source during aircraft approach [1] and many studies for the trailing-edge flow and noise have been conducted from various view points, for example such as Ref. [2]-[6]. However, the mechanism of the noise generation at the trailing edge of an airfoil is not fully understood.

The author is developing a new high-resolution numerical method to solve the Navier-Stokes equations [7]. During the validation of the method, an interesting flow feature was observed as shown in Fig.1. On the upper surface of the slat, the boundary layer becomes turbulent just after the suction peak. If we observe it by the density distribution, the unsteady flow on the upper surface is shown as a number of small vortices rolling downward along the surface. When these vortices leave from the trailing edge, they strongly interact with the flow from the lower surface due to the large pressure difference between the upper and lower surfaces.

The result of Fig.1 is a two-dimensional computation, while the Reynolds number of this flow is Re=2.83x10^6 so that most part of the airfoil surfaces must be covered by turbulent boundary layers where the three-dimensionality is essential. Therefore, to discuss the flow physics from two-dimensional computations

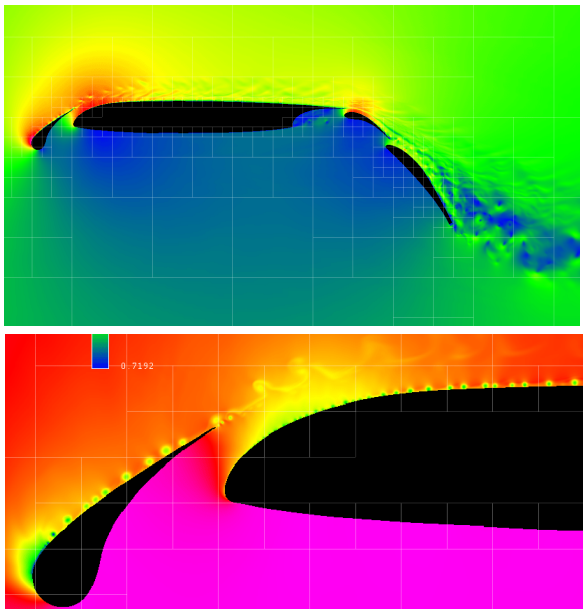

Fig.1 Instantaneous Mach (upper) and density (lower) distributions of NASA supercritical four-element airfoil at Re=2.83x10^6, Freestream Mach number=0.201, and angle of attack=8.16 degrees. The time-averaged Cp distribution shows good agreement with the experiment.

may mislead the conclusion. However, it is certain that the interaction of vortices at the trailing edge is important for understanding the trailing-edge noise source.

The objective of this paper is to investigate the flow in the vicinity of the trailing edge of an airfoil in detail using the high-resolution CFD. In order to focus on understanding the vortex motion near the airfoil trailing edge, a relatively lower Reynolds number is employed in the present computations. With a lower Reynolds number, the flow around an airfoil is essentially two-dimensional even with separated boundary layers [8]. The lower Reynolds number also enables the direct numerical simulation (DNS) which is required to observe the vortex motions.

2 Numerical Method

2.1 Approach

In the present study, an approach named the Building-Cube Method (BCM) [7] was used to compute the flow field. This approach was developed aimed for direct numerical simulation around real geometries with an expectation of near-future high-performance computers.

In the BCM, a flow field is described as an assemblage of building blocks of cuboids, named 'Cube' as shown by red lines in Fig.2(a). Each cube is a sub-domain of the flow computation and an equally-spaced fine Cartesian mesh is used in it. All cubes have the same number of grid points so as to simplify the parallel computations. The geometrical size of each cube is determined by adapting to the geometry and the flow features so as to fit the grid spacing to the local flow scale. The use of the Cartesian grid in each cube allows a simple treatment of complex geometries and an easy implementation of higher-order numerical schemes.

2.2 Numerical method

A non-dimensional form of the compressible Navier-Stokes equations can be written in the Cartesian coordinates x_j, (j=1, 2, 3) as

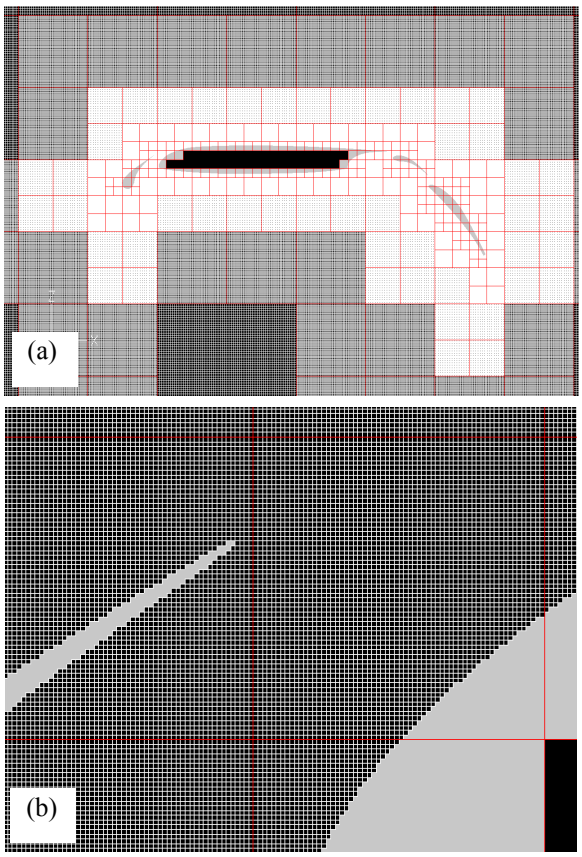

Figure 2. BCM mesh for a four-element airfoil. (a) Cube boundaries (red lines). (b) Cartesian mesh near the wall, drawn for every four lines.

$$\frac{\partial \mathbf{Q}}{\partial t}+\frac{\partial \mathbf{F}_j}{\partial x_j}-\frac{1}{Re}\frac{\partial \mathbf{G}_j}{\partial x_j}=0, \qquad (1)$$

where $\mathbf{Q}=[\rho,\rho u,\rho v,\rho w,e]^T$ is the vector of conservative variables, ρ is the density, u, v, w are the velocity components in the x, y, z directions and e is the total energy. The vectors $\mathbf{F}(\mathbf{Q})$ and $\mathbf{G}(\mathbf{Q})$ represent the inviscid and viscous flux vectors respectively, and Re is the Reynolds number.

The compressible Navier-Stokes equations are solved by a cell-centered, finite-volume scheme on an equally-spaced Cartesian mesh. For a cube-k, the Cartesian mesh spacing Δx_k in the cube is simply given by $\Delta x_k=\Delta s_k/n_{\text{cell}}$ where Δs_k is the size of the cube-k and n_{cell} is the number of cells along each coordinate in a cube. The number of cells, n_{cell}, is same in x, y and z directions in three-dimensional computations. However, for two-dimensional computation

shown in this paper, n_{cell} in y-coordinate is set to be 3 in order to compute a two-dimensional field by the three-dimensional flow solver.

An algebraic form of the equation (1) can be written as follows,

$$\frac{\partial \mathbf{Q}_i}{\partial t} = -\frac{1}{\Delta x_k}\left[\sum_{j(i)}^{6}\mathbf{h}\left(\mathbf{Q}_{ij}^{+},\mathbf{Q}_{ij}^{-},\mathbf{n}_{ij}\right) - \frac{1}{Re}\sum_{j(i)}^{6}\mathbf{G}\left(\mathbf{Q},\mathbf{n}_{ij}\right)\right], \quad (2)$$

where the summation $j(i)$ means all six faces around the regular hexahedron cell-i. The term $\mathbf{h}(\mathbf{n}_{ij})$ is an inviscid numerical flux vector normal to the control volume boundary, and $\mathbf{Q}_{ij}^{+}, \mathbf{Q}_{ij}^{-}$ are values on both sides of the control volume boundary. The numerical flux $\mathbf{h}$ is computed using an approximate Riemann solver of HLLEW (Harten-Lax-van Leer-Einfeldt-Wada) [9]. The primitive variables on the cell interface are evaluated by the fourth-order compact-like MUSCL scheme [10].

The lower/upper symmetric Gauss-Seidel (LU-SGS) implicit method is used for the time integration. In order to keep the time accuracy, a sub-iteration scheme [11] developed for the higher-order time accuracy is employed.

Body boundaries is defined by a staircase representation as shown in Fig. 3 in order to keep the simplicity of the algorithm and to minimize the memory requirement per node. Although an excessively fine mesh is required to keep the geometrical accuracy for curved boundaries, the flow physics in the boundary layers also requests the fine mesh to resolve small vortices.

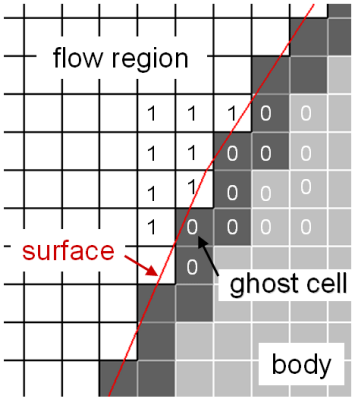

Fig. 3. Ghost cells at body boundary.

Each computational cell in a cube has a flag value depending on the location; flag of 1 in the flow field and 0 in the body. The body boundary is defined by the cell boundaries between adjacent cells having different flag values. Ghost cells are defined as those cells that locate in the body and next to the flow field. Boundary conditions are assigned to these ghost cells.

Wall boundary conditions of density and pressure are given at the ghost cell as average values of the surrounding cells by the following manner.

$$g_{\text{ghost}} = \sum_{i(\text{adjacent cells})}\left(g_i \times flag_i\right) \Big/ \sum_{i(\text{adjacent cells})}\left(flag_i\right). \quad (3)$$

Here the value of g is density or pressure and the *flag* is 0 for a cell in the body and 1 in the flow field. With this boundary condition, information of the wall normal is not required. This simplifies the grid data and the solution procedure, although very fine mesh must be used at wall boundaries. The velocity components at these ghost cells for the solid wall boundary are set to be zero.

At cube boundaries, information exchanges are required between adjacent cubes. The simplicity of the algorithm is also kept by using ghost cells at the cube boundaries. At each side of cube, three ghost cells are added beyond the cube boundary. Therefore, if the sizes of two adjacent cubes are same, the exact overlapping of six cells at cube boundary ensures the accurate transfer of the information up to the fourth-order special accuracy. The information transfer from smaller cube to larger one is performed by assigning the average values of smaller cube near the boundary. The transfer from the larger cube to smaller one is by just taking the value in the larger cells. Cube-boundary values are updated by sub-iterations to keep the time accuracy.

The flow solver was parallelized using the OpenMP library for sheared-memory parallel computers, by simply distributing the cubes to the CPUs in a sequential manner.

3 Numerical Results

3.1 Computational conditions

In the present study, NACA0012 airfoil at relatively low Reynolds number was used to observe the vortex motions near the airfoil trailing edge. The computed Reynolds number is 50,000 based on the chord length and the free stream Mach number is 0.5. The angles of attack were changed from zero to five degrees. With this Reynolds number, the flow along the airfoil surface is essentially laminar [8] so that the two-dimensional computations were performed for the present study. No turbulence models were used.

The number of cubes is 522, and each cube has 64x64 Cartesian mesh in it. Therefore, the total number of computational cells is 522x64x64 =2,138,112. The minimum spacing in the near-wall cube is 4.58×10^{-4} to the chord length. Outer boundary is located at 60 chord length.

3.2 Computed results

A. Angle of attack of 1 degree

Figure 4 shows the computed Mach contours around the NACA0012 airfoil at angle of attack of 1 degree. At this angle of attack, there is no separation and the flow is steady. The similar steady flow results were obtained at angles of attack from zero to two degrees.

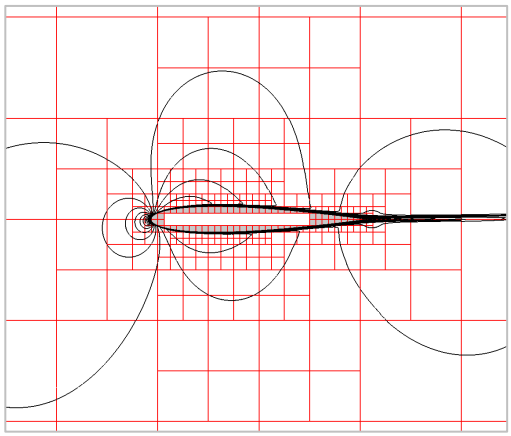

Fig. 4 Computed Mach contours at $\alpha = 1°$

B. Angle of attack of 3 degrees

In Fig.5, instantaneous density distributions around NACA0012 airfoil are drawn with a certain interval. Figure 6 are the corresponding pressure distributions.

The laminar boundary layer on the upper surface separates at mid-chord and generates vortices that flows down along the airfoil surface. When a vortex reaches at the trailing edge, it generate a small counter-rotating vortex. At the same time a pressure wave is generated that propagates in all directions from the trailing edge. This observation from the computed results may show the mechanism of the trailing edge noise generation.

The generation of the pressure wave at the trailing edge is caused by two important items. One is the vortex and the other is the sharp trailing edge. The vortex generated at the separated boundary layer induces clockwise flow around it. When the vortex reaches at the trailing edge, the induced flow by the vortex hit the undersurface near the trailing edge region. Due to the high pressure on the lower surface and the low pressure at the center of the vortex along with the sharp convex configuration at the trailing edge, a counter-rotating vortex is generated. With this sudden creation of a vortex generates the pressure wave.

There may exist a feedback loop in this phenomena. The laminar boundary layer on the upper surface of the airfoil separates at the mid-chord region. This separated shear layer has an inherent instability. However, for the present case, the vortex generation from the separated shear layer seems to be triggered by the pressure wave originated at the trailing edge as schematically shown in Fig. 7.

Let the sound speed be a, then the propagation velocity toward the upstream direction from the trailing edge is given by $v = a - u$, where u is the flow velocity near the airfoil surface. Let the distance between the separation point and the trailing edge be s, then the time of travel of the pressure wave from the trailing edge to the separation point is s/v. Since the velocity of the vortex movement along the airfoil surface is equal to the local flow velocity u, the time of travel over the feedback loop must

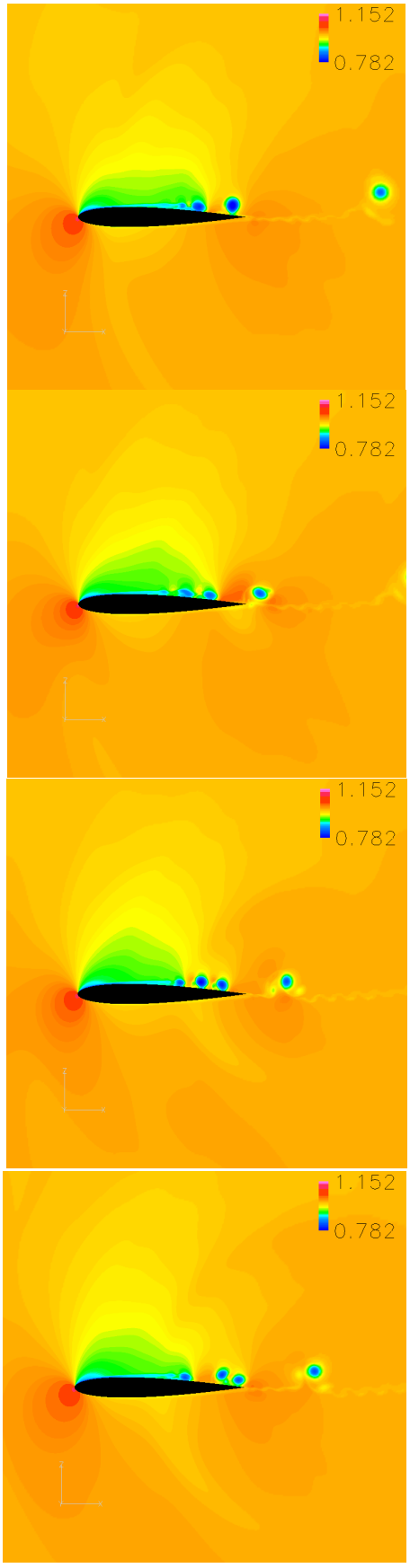

Fig. 5 Density distribution at α=3°

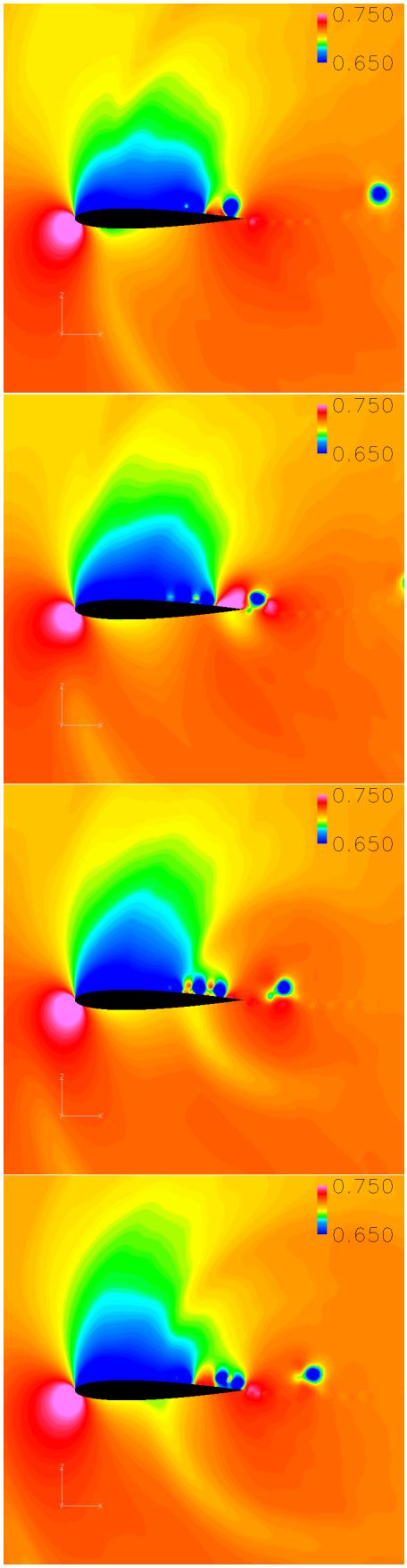

Fig. 6 Pressure distribution at α=3°

be equal to an integral number of the period of oscillation T. This yields

$$\frac{s}{a-u}+\frac{s}{u}=nT\ , \quad n=1, 2, 3, \ldots \qquad (4)$$

The frequency of the trailing edge noise f is given by

$$f=\frac{n(a-u)u}{as}, \quad n=1, 2, 3, \ldots \qquad (5)$$

For the simplicity, let's assume that the local flow velocity u can be approximated by freestream velocity. Then, Eq. (4) can be written as

$$nT=\frac{s}{a}\cdot\frac{1}{M_\infty(1-M_\infty)} \qquad (6)$$

where M_∞ is the freestream Mach number. Then the nondimensional time is

$$\tilde{T}=\frac{T}{a/c}=\frac{s}{nc}\cdot\frac{1}{M_\infty(1-M_\infty)} \qquad (7)$$

The length of separation region s of the present case is about $0.5c$ where the c is the chord length. Then, the nondimensional time at $M_\infty=0.5$ is 2/n. The nondimensional time obtained by the simulation shown in Fig. 5 and 6 is 1.2 which is very close to the value

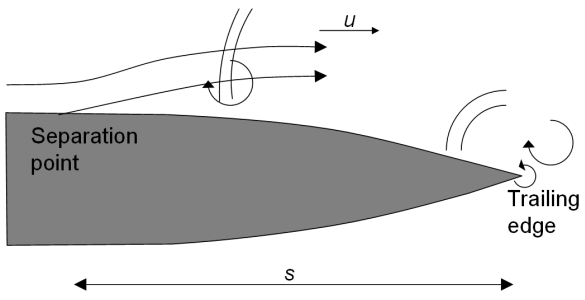

Fig. 7 Feedback loop

computed by Eq. (7) with n=2. This means that the trailing edge tone of this computed case has the feedback loop.

C. Effects of trailing edge modifications

Since the trailing edge noise is generated by the interaction of vortex at the sharp trailing edge, modification of airfoil geometry near the trailing edge may be effective to weaken the noise generation. In the present study, three modifications were employed as shown in Fig. 8. The first one shown in Fig.8(a) is a slit of 0.01c width at 0.9 chord length. The second one of Fig.8 (b) is a small upward plate of 0.02 chord height at the trailing edge. The third one, Fig. 8(c), is the downward plate. These modifications are very easy in the present computation because of the Cartesian grid.

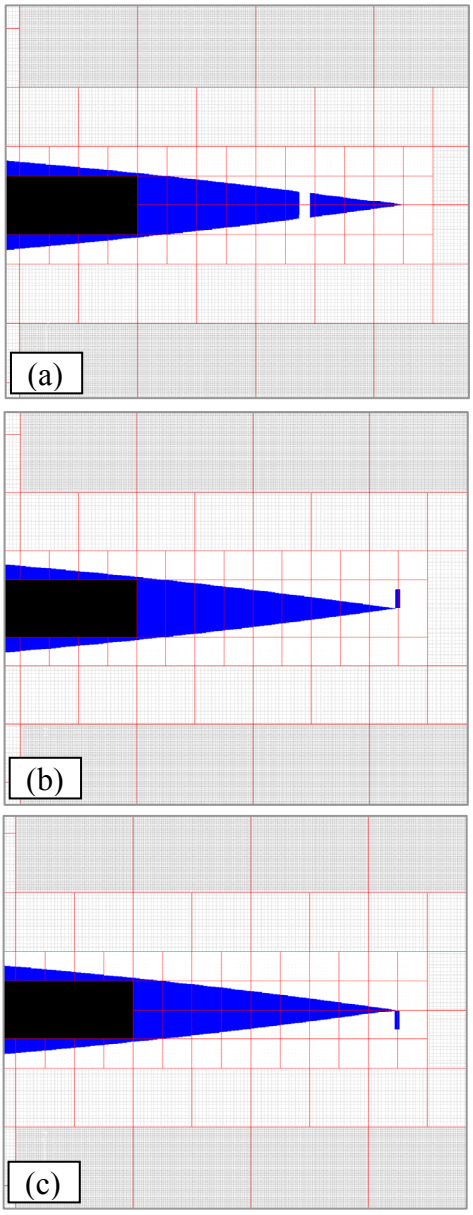

Fig.8 Trailing edge modifications

If there is a narrow slit near the trailing edge, the pressure difference between the upper and lower surfaces of the airfoil induces flow through the slit. This jet-like flow can be expected to be effective to weaken the vortex on the upper surface. However, the computed results in Fig. 9 did not show any improvement. More study to find optimum location, direction and width of the slit is required for the effective reduction of the trailing edge noise by slits.

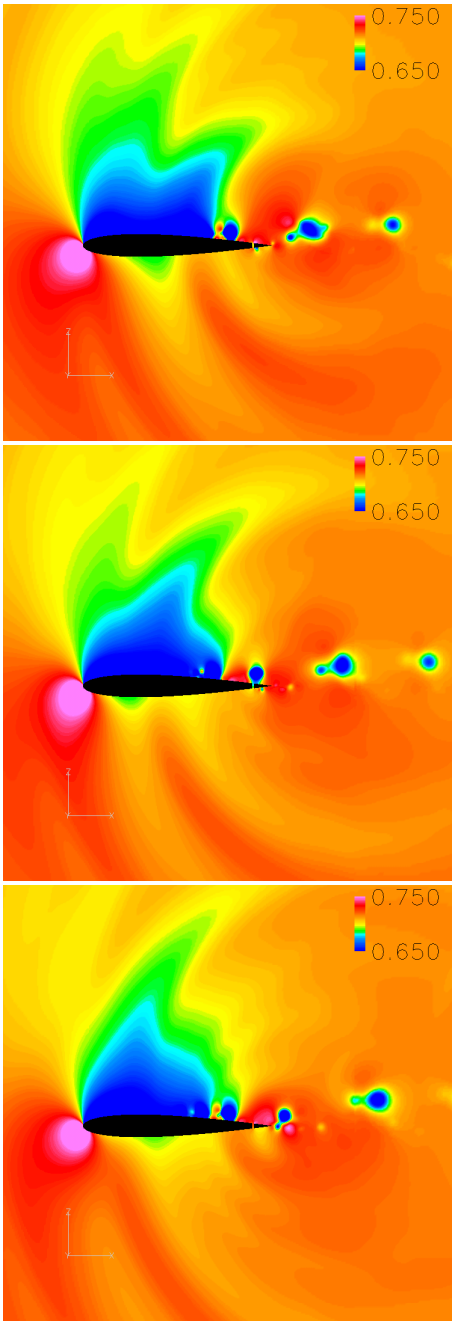

Fig. 9 Computed pressure distributions for an airfoil with a slit (Fig.8-a) at α=3°.

Computed pressure distributions around an airfoil with a small end plate at the trailing edge are shown in Fig. 10 and 11. The upward end plate of Fig.8(b) is shown in Fig.10 and the downward end plate of Fig.8(c) is shown in Fig. 11. With these end plates,. the frequencies of the vertical shedding are increased, and the strength of each vortex became smaller. This is due to the more complex interaction occurred at the crank-shaped trailing edge.

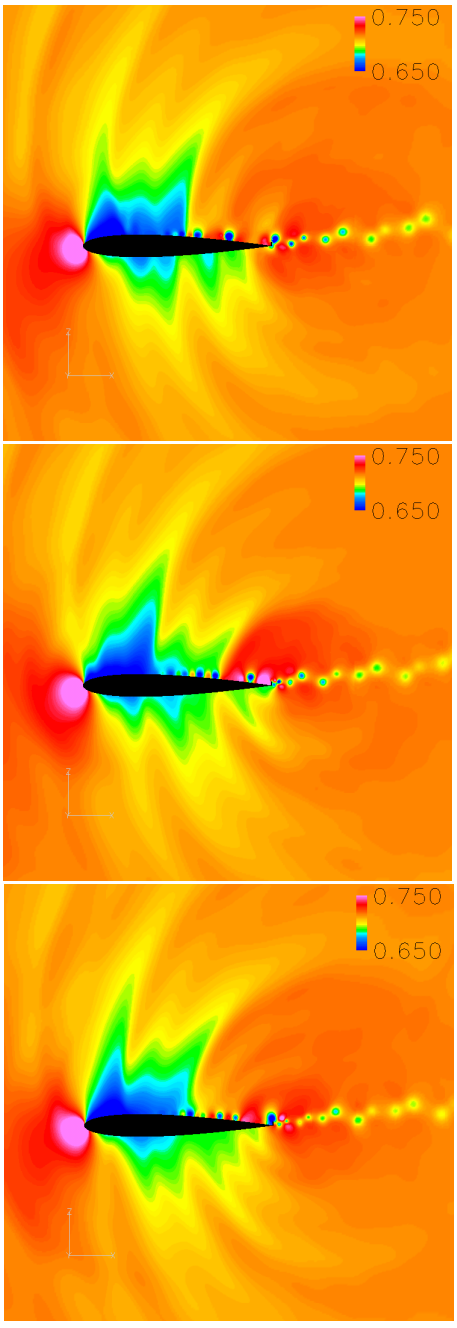

Fig. 10 Computed pressure distributions for an airfoil with upward end plate (Fig.8-b) at α=3°.

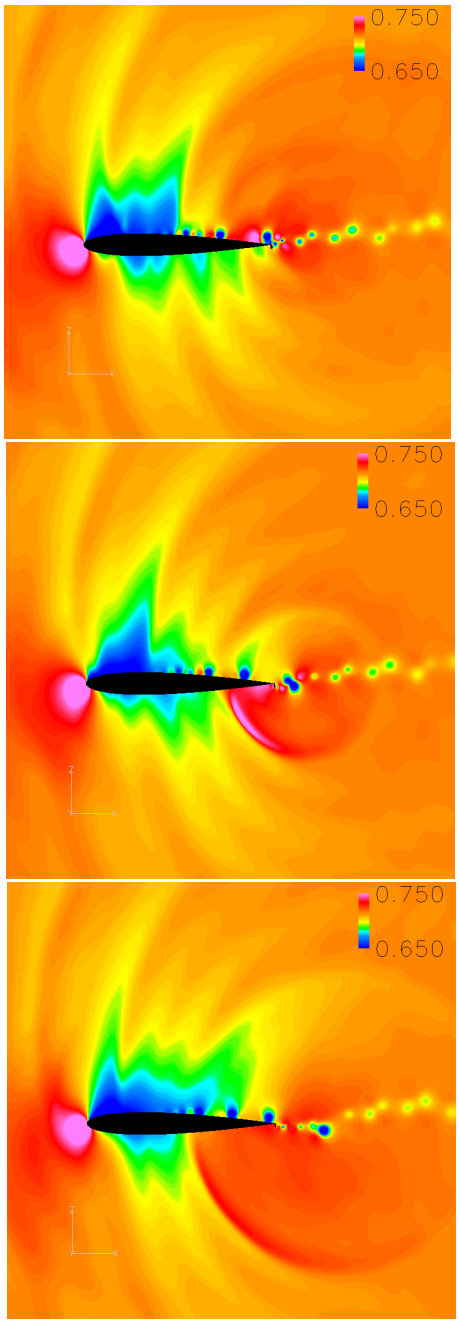

Fig. 11 Computed pressure distributions for an airfoil with downward end plate (Fig.8-c) at α=3°.

By comparing the upward and downward end plates, the former is more effective to reduce the trailing edge noise. However, the upward trailing edge will reduce the lift as well.

4 Conclusion

Flows around NACA0012 airfoil at relatively low Reynolds number were numerically simulated using a high-resolution numerical method named Building-Cube method.

From an animation of the computed data around NACA airfoil, it was shown that the laminar boundary layer on the upper surface separated and periodically generated vortices. When a vortex reached at the trailing edge of the airfoil, it generated a counter-rotating vortex and produced a pressure wave. There seems to exist a feedback loop between the vortex generation near the separation point and the pressure wave originated at the trailing edge.

Among the modifications of the trailing edge, the upward end plate was most effective for weakening the trailing edge noise with the present flow conditions. It is certain that the trailing edge noise can be reduced with a proper modification of the airfoil shape near the trailing edge. The present computational approach named Building-Cube method is very useful for investigating the flow field with these small modifications of the wall boundaries.

The computations in this study are for laminar flows at relatively low Reynolds number. In real world, the Reynolds number is much higher and the boundary layers are turbulent. Therefore, the future work of the present study is three-dimensional computations.

Acknowledgments

The computations were carried out on the NEC SX-7 at the Super-Computing System of Information Synergy Center and the SGI Altix of the Advanced Fluid Information Research Center, Institute of Fluid Science, Tohoku University.

References

[1] Soderman, P. T., Kafyeke, F., Boudreau, J., Chandrasekharan, R., “Airframe noise study of Bombardier CRJ-700 aircraft model in the NASA Ames 7- by 10-foot wind tunnel,” Int. J. Aeroacoustics, Vo.3, No.1, pp.1-42, 2004.

[2] Yu, J. C., and Tam, C. K. W., “Experimental Investigation of the Trailing Edge Noise Mechanism,” AIAA J., Vol.16, No.10, pp.1046-1052, 1978.

[3] Wang, M. and Moin, P., “Computation of Trailing-Edge Flow and Noise Using Large-Eddy

Simulation," AIAA J., Vol.38, No.12, pp.2201-2209, 2000.

[4] Tam, C. K. W., and Pastouchenko, N., "Gap Tones," AIAA J., Vol.39, No. 8, pp. 1442-1448, 2001.

[5] Khorrami, M. R., Singer, B. A., and Berkman, M. E., "Time-Accurate Simulations and Acoustic Analysis of Slat Free Shear Layer," AIAA J., Vol. 40, No. 7, pp.1284-1291, 2002.

[6] Herr, M., and Dobrzynski, W., "Experimental Investigations in Low-Noise Trailing-Edge Design," AIAA J., Vol.43, No.6, pp.1167-1175, 2005.

[7] Nakahashi, K., "High-Density Mesh Flow Computations with Pre-/Post-Data Compressions," 17th AIAA CFD Conference, Toronto, AIAA 2005-4876, 2005.

[8] Elimelech,Y., et. al., "On the Onset of Transition at Low Reynolds Number Flow Over Airfoils," 4th AIAA Theoretical Fluid Mechanics Meeting, Toronto, AIAA 2005-5311, 2005.

[9] Obayashi, S., Guruswamy, G. P., "Convergence Acceleration of a Navier-Stokes Solver for Efficient Static Aeroelastic Computations," *AIAA Journal*, Vol.33, No.6, pp.1134-1141, 1995.

[10] Yamamoto, S., Daiguji, H., "Higher-Order-Accurate Upwind Schemes for Solving the Compressible Euler and Navier-Stokes Equations," *Computer and Fluids*, Vol.22, No.2/3, pp.259-270, 1993.

[11] Matsuno, K., "Improvement and Assessment of an Arbitrary-Higher-Order Time-Accurate Algorithm," *Computer and Fluids*, Vol.22, No.2/3, pp.311-322, 1993.